PROCEEDINGS, Thirty-Sixth Workshop on Geothermal Reservoir Engineering
Stanford University, Stanford, California, January 31 - February 2, 2011
SGP-TR-191

AN APPROACH TO MODELING COUPLED THERMAL-HYDRAULIC-CHEMICAL PROCESSES IN GEOTHERMAL SYSTEMS

Jennifer Palguta[1], Colin F. Williams[1], Steven E. Ingebritsen[1], Stephen H. Hickman[1], and Eric Sonnenthal[2]

[1]U.S. Geological Survey
345 Middlefield Rd, MS 977
Menlo Park, CA, 94025, USA
e-mail: jpalguta@usgs.gov

[2]Lawrence Berkeley National Laboratory
1 Cyclotron Road
Berkeley, CA, 94720, USA

ABSTRACT

Interactions between hydrothermal fluids and rock alter mineralogy, leading to the formation of secondary minerals and potentially significant physical and chemical property changes. Reactive transport simulations are essential for evaluating the coupled processes controlling the geochemical, thermal and hydrological evolution of geothermal systems. The objective of this preliminary investigation is to successfully replicate observations from a series of hydrothermal laboratory experiments [Morrow et al., 2001] using the code TOUGHREACT. The laboratory experiments carried out by Morrow et al. [2001] measure permeability reduction in fractured and intact Westerly granite due to high-temperature fluid flow through core samples. Initial permeability and temperature values used in our simulations reflect these experimental conditions and range from 6.13×10^{-20} to 1.5×10^{-17} m^2 and 150 to 300 °C, respectively. The primary mineralogy of the model rock is plagioclase (40 vol.%), K-feldspar (20 vol.%), quartz (30 vol.%), and biotite (10 vol.%). The simulations are constrained by the requirement that permeability, relative mineral abundances, and fluid chemistry agree with experimental observations. In the models, the granite core samples are represented as one-dimensional reaction domains. We find that the mineral abundances, solute concentrations, and permeability evolutions predicted by the models are consistent with those observed in the experiments carried out by Morrow et al. [2001] only if the mineral reactive surface areas decrease with increasing clay mineral abundance. This modeling approach suggests the importance of explicitly incorporating changing mineral surface areas into reactive transport models.

INTRODUCTION

The search for sources of renewable energy has promoted interest in geothermal energy exploration and development. Interactions between hydrothermal fluids and rock alter the primary mineralogy, leading to formation of secondary minerals and potentially significant physical and chemical property changes [Xu and Pruess, 2001; Xu et al., 2003]. Reactive transport simulations provide an objective and systematic means of investigating and evaluating the competitive interactions between fluids and rock-forming minerals over space and time for a range of conditions [Steefel et al., 2005]. However, endeavors to model coupled thermal-hydrologic-chemical (THC) processes are complicated by the number of poorly constrained processes that occur under hydrothermal conditions. In order to maximize their utility, reactive transport models must adequately integrate the various fundamental processes that control system properties and evolution.

A major challenge in the field of reactive transport modeling has been the development of general models that will transfer to different geothermal sites and conditions. The many assumptions, uncertainties, and approximations intrinsic to reactive transport models restrict our ability to draw general conclusions regarding the behavior of natural geothermal systems. Although hydrothermal fluids and rocks interact under a diverse range of conditions, most studies necessarily present simulation results that are specific to a particular set of conditions and parameters [e.g., Xu and Pruess, 2001; Xu et al., 2001; Maher et al., 2006]. If reactive transport models are to be more broadly applied to problems such as the analysis and exploration of geothermal systems, then these models must be transferable from one system to another (i.e., not site specific). This requires modeling techniques that are

sufficient enough to apply over a wide-range of conditions.

Reactive transport models rely on mathematical formulations to describe the coupled THC processes occurring in hydrothermal environments [Johnson et al., 1998]. The general mathematical expression typically used to predict mineral dissolution or precipitation rates is based on transition state theory and has the form [Aagaard and Helgeson, 1982; Helgeson et al., 1984; Lasaga, 1984]:

$$rate = A \cdot k \cdot f(\Delta G) \quad (1)$$

where A is the specific reactive surface area, k the rate constant, and $f(\Delta G)$ a function which gives the dependence of the rate on the Gibbs free energy (ΔG). Equation (1) illustrates the overall rate dependence on: (i) the proximity to equilibrium (i.e., the degree of saturation, which is defined in terms of the Gibbs free energy), (ii) rate constants, and (iii) mineral surface areas. Changes to any of these terms can contribute to significant differences in the predicted mineral dissolution/precipitation behavior and, by extension, the evolution and behavior of the system. Comparisons of various studies [e.g., Martin and Lowell, 1997; Johnson et al., 1998; White and Brantley, 2003; André et al., 2006; Maher et al., 2006; Yasuhara and Elsworth, 2006] indeed indicate that differences in kinetics, surface area, solution chemistry, and mineral composition and solubility can cause significant differences in predicted mineral precipitation and permeability evolution. Therefore, in addition to appropriate mathematical formulations of the coupled processes, reactive transport models require accurate compositional, thermodynamic, and kinetic data. Unfortunately, values for parameters such as mineral compositions and solubilities, fluid chemistry, rate constants, and reactive surface areas are often difficult to constrain or unavailable [White and Peterson, 1990; Alekseyev et al., 1997; Cama et al., 2000; Brantley, 2003; Maher et al., 2006].

The multitude of unconstrained variables presents a significant challenge. For the purposes of this study, we have reduced the problem to a more tractable size by focusing on the numerical treatment of reactive surface areas. Although all the parameters mentioned above introduce uncertainty into reactive transport models, mineral surface areas remain one of the most uncertain and poorly quantified parameters [White and Brantley, 1995; Bethke, 1996; Alekseyev et al., 1997; Cama et al., 2000; Steefel, 2001; Lasaga and Lü□ttge, 2003; Xu et al., 2004a; Maher et al., 2006; Brantley, 2003, 2008]. Relatively few studies have attempted to simulate physical changes in mineral surface areas or to evaluate their effects on dissolution and precipitation rates [Sonnenthal and Ortoleva, 1994; Brantley and Conrad, 2008]. Surface areas are notoriously difficult to ascertain [Nagy et al., 1991; Nagy and Lasaga, 1992; Stillings and Brantley, 1995; Amrhein and Suarez, 1992; Ganor et al., 1995, 1999; Cama et al., 2000] and are known to change with time due to poorly quantifiable phenomena. Processes affecting reactive surface area include coating of reactive mineral phases by other, less reactive minerals (armoring), dissolution pitting and etching, and creation of isolated porosity through crack healing and sealing [Brantley et al., 1990; Chester et al., 1993, Brantley, 2003; Brantley and Conrad, 2008]. The findings of White and Brantley [2003] and Maher et al. [2006] indicate that these changes in mineral surfaces may significantly contribute to the observed changes in rates.

Using the popular fluid flow and geochemical transport code TOUGHREACT [Xu and Pruess, 1998; Xu et al., 2004a], we present a relatively straightforward method for representing the progressive loss of reactive surface area due to occlusion by secondary precipitates. Since a critical benchmark for any numerical model is accurate simulation of well-constrained experiments, model success is predicated on agreement with a series of flow-through laboratory experiments conducted on cylindrical samples of Westerly granite at temperatures from 150 to 300 °C [Morrow et al., 2001]. Both intact and fractured granitic samples were used in the experiments, resulting in a range of initial permeability values. The objective of this preliminary investigation is to evaluate the use of a one-dimensional model that explicitly considers the temporal evolution of reactive surface areas for simulating the physical and chemical evolution of fractured granite under various hydrothermal conditions. The results presented in this paper can be compared to results from more complex multi-dimensional models. The intent is to better quantify and characterize the processes dominating the evolution of natural geothermal systems. Because rates are controlled by a combination of factors, an improved mechanistic or process-based understanding should facilitate the future development and utility of these models for field applications.

SURFACE AREA EFFECTS

Modeling reaction rates and their subsequent effects on system evolution requires knowledge of the total mineral surface areas in contact with the aqueous phase. The surface area, A, used in Eq. (1) typically is based on either gas adsorption measurements (BET) or geometric estimates [Maher et al., 2006; Brantley and Conrad, 2008]. However, BET surface areas are consistently higher than those based on geometric estimates [Dorn, 1995; Brantley et al., 1999; White and Brantley, 2003]. Additionally, there are substantial uncertainties associated with both

Table 1: Summary of experiments from Morrow et al. [2001].

Name	Sample Type	Temperature (°C)	Initial Permeability ($m^2 \times 10^{-21}$)	Final Permeability ($m^2 \times 10^{-21}$)
150i	intact	150	63.2	55.6
250i	intact	250	61.3	29.3
250f-1	fractured	250	129.0	16.7
250f-2	fractured	250	6900.0	980.0
300i	intact	300	166.1	59.1
300f	fractured	300	15081.7	581.7

approaches for assigning reactive surface area [e.g., Gautier et al., 2001; Brantley, 2003; Zhu, 2005; Maher et al., 2006; Peters, 2009]. It has been noted that coatings commonly form on mineral surfaces over time and can cause significant variations between initial and final surface areas [Cama et al., 2000; Brantley, 2003; Peters, 2009]. Furthermore, these surface coatings are reported to develop early and rapidly [Banfield and Barker, 1994; Nugent et al., 1998]. These previous studies indicate that the accumulation of clay minerals in pore spaces and on grain surfaces can be very effective at reducing the fraction of reactive minerals accessible to the fluid. Consequently, decreases in rates of primary mineral depletion and secondary mineral formation are likely partially attributable to reductions in reactive surface areas [White and Brantley, 2003]. This argues that the progressive occlusion of the reactive mineral substrate must factor into prediction of reaction rates. Thus, accounting for the development of such mineral coatings may help to facilitate more accurate predictions [Dove , 1995; Cama et al., 2000; Peters, 2009].

LABORATORY EXPERIMENTS

Here we provide a brief description of the experiments simulated in this study. Additional details can be found in Morrow et al. [2001] and references therein. In order to assess changes in permeability, mineralogy, and solute concentrations, Morrow et al. [2001] conducted high-temperature flow-through experiments on cylinders of intact or fractured (split) Westerly granite measuring 18.0 mm in diameter and 38.1 mm in length, with fractures in the latter type of experiment oriented parallel to the cylinder axis. The experiments were conducted at an effective pressure of 50 MPa and at temperatures from 150 to 500 °C (only experiments ≤ 300 °C were considered in the numerical models). A pore-pressure differential of 2 MPa was imposed across the length of the sample, producing a steady-state flow regime. Experiments were started using distilled water. The pore fluid was cycled back and forth at intervals of approximately 10,000 to 40,000 seconds by reversing the 2 MPa fluid pressure gradient. Consequently, the same fluid, with an evolving chemical composition, flowed back and forth through each sample over time.

Morrow et al. [2001] measured total flow and total pressure drop across the samples and reported an average or apparent permeability for each sample on the basis of overall column dimensions. The reported permeability values were calculated according to Darcy's law:

$$Q/A_{csa} = p/\mu(dP/dx) \tag{2}$$

where Q is volumetric flow rate, A_{csa} is the cross-sectional area of the sample, p is permeability, μ is the dynamic viscosity of water at the temperature and pressure of the experiment, and (dP/dx) is the pore fluid pressure gradient across the sample. The lower limit for the permeability measurements was 1×10^{-22} m^2. The authors observed that after an initial stage of rapid permeability loss, experiments generally reverted to a state in which permeability followed an exponential decay in time. Pore fluid was extracted for chemical analysis at the conclusion of one experiment conducted on a fractured sample at 250 °C (250f-2 in Table 1). This fluid was analyzed for major cations and silica. Unfortunately, fluids could not be sampled during the experiments without adversely affecting the fluid pressure and chemistry. Therefore, only a final composition is available from a single sample for comparison with model results. The mineralogy of selected fractured samples was also examined before and after alteration and the relative abundances were reported. In order of decreasing abundance, the newly crystallized minerals observed at 150 °C are Fe-rich smectite, K-feldspar, albite, quartz, calcite, and Ca-Al zeolite. Similarly, at 250 °C the observed secondary minerals are smectite, calcite, K-feldspar, albite, quartz, Ca-Al zeolite.

REACTIVE TRANSPORT MODEL

Governing Equations

Simulations of the flow-through experiments were carried out using the code TOUGHREACT [Xu and Pruess, 1998; Xu et al., 2004a]. Here, we outline the standard equations used in the code to model fluid and heat flow, chemical transport, and reactions. We also discuss the modified equations used for calculating surface area changes. The primary governing equations for multiphase fluid and heat flow and chemical transport have the same structure. These equations are derived from the conservation laws for mass, energy, and momentum. In general, the flow and transport equations are expressed as [Xu et al., 1997, 2004a]:

$$\frac{\partial M_i}{\partial t} = -\nabla \cdot \mathbf{F}_i + q_i \tag{3}$$

where M is the mass accumulation, **F** the mass flux, and q a source/sink term. The subscript i represents either fluid, heat, or aqueous chemical components. The primary governing equations are coupled to constitutive local relationships that express all parameters as functions of fundamental thermo-physical and chemical variables.

The equations for kinetically-controlled mineral dissolution and precipitation are given using a general form of rate law [Lasaga, 1984; Steefel and Lasaga, 1994; Palandri and Kharaka, 2004]:

$$r_j = A_j k_j \left[1 - \left(\frac{Q_j}{K_j} \right)^{\theta} \right]^{\eta} \tag{4}$$

where r_j is the dissolution/precipitation rate (positive values indicate dissolution and negative values precipitation), A_j the specific reaction surface area per kg_{H2O}, k_j the rate constant, K_j the equilibrium constant for the mineral-water reaction, Q_j the ion activity product, and the subscript j the mineral index. The exponents θ and η are experimentally determined parameters. In this study, they are taken to be equal to one for all mineral components, j, in the system. The rate constant is a function of temperature, approximated by:

$$k = k_{25} \exp\left[\frac{E_a}{R} \left(\frac{1}{T} - \frac{1}{298.15} \right) \right] \tag{5}$$

where E_a is the activation energy, k_{25} the rate constant at 25 °C, R the gas constant, and T temperature (K). These mathematical representations of mineral reaction kinetics determine the physical and chemical evolution of the model system.

TOUGHREACT can also track temporal changes in porosity and permeability due to mineral dissolution and precipitation. Changes in porosity are calculated from changes in mineral volume fractions. The code offers several options for calculating changes in permeability. For example, permeability change can depend on porosity change [Steefel and Lasaga, 1994] or on fracture aperture change [Snow, 1968; Xu et al., 2004a]. Since fluid flow in low-porosity crystalline rocks typical of geothermal fields is dominated by fractures (both at the macroscopic and microscopic scales), the following expression is used to relate permeability changes to changes in hydraulic aperture:

$$p = \frac{\left(b_o + \Delta b \right)^3}{12 s} \tag{6}$$

where p is permeability, b the hydraulic aperture, Δb the aperture change resulting from mineral precipitation/dissolution, and s the fracture spacing. The subscript o indicates the initial value.

Several theoretical models have been proposed to relate changes in porosity, φ, to changes in specific surface area, A [Kieffer et al., 1999; Emmanuel and Berkowitz , 2005]. These models often are based on simple geometric considerations assuming a porous media, such as sandstone, consisting of an array of spherical pores and have the form:

$$A = A_o \left(\frac{\phi}{\phi_o} \right)^{2/3} \tag{7}$$

However, such models remain largely unverified and may not be appropriate for fractured rock [Emmanuel and Berkowitz, 2005]. For the purposes of this study, we related changes in surface area to changes in fracture permeability using:

$$A = A_o \left(\frac{p}{p_o} \right)^{n} \tag{8}$$

where n is a numerically determined fitting parameter that can either be constant or given by:

$$n = l \left[1 - \left(\frac{\Delta_{clay}}{\phi_o} \right)^{m} \right] \tag{9}$$

where Δ_{clay} is the change in smectite abundance expressed as the volume fraction of clay relative to total rock volume. The parameters n, l, and m were selected to provide the best match to the experimental observations. Although Eqs. (8) and (9) do not derive directly from first-principle theory or geometric arguments, as discussed in more detail below, these equations were implemented as one way of representing the physical process of reactive surface area reduction due to clay mineral precipitation (i.e., armoring). As previously discussed, when clays precipitate along a fracture wall they cause a reduction in reactive surface area (Eq. 8). However, after an initial clay-mineral coating forms, this mechanism of physical occlusion may become less important for controlling reaction rates. This decreasing control is not simulated by Eq. (8) using a constant n. In Eq. (9), as smectite fills the void space, (Δ_{clay}/φ_o) goes to 1 and n goes to 0. Consequently, Eq. (9) is used to evaluate the control of physical occlusion by clay minerals on reaction rates (Eq. 4) over time. As discussed in detail below, use of Eq. (8) with either constant n or variable n (Eq.

9) to simulate changes in reactive surface area provides a much better fit of our model results to the experimental observations of Morrow et al. [2001] than can be obtained assuming a constant *A*.

Model Description and Setup

A total of six experiments performed by Morrow et al. [2001] were simulated in this study and have been designated 150i, 250i, 250f-1, 250f-2, 300i, and 300f. Details on the experimental configurations are listed in Table 1. These experiments consisted of both intact (i) and fractured (f) cylindrical samples of Westerly granite at temperatures ranging from 150 to 300 °C. The granite cylinders were represented as a one-dimensional reaction domain using a 76 volume element mesh with dimensions and interface areas identical to those of the cylinders. Additionally, two large-volume elements are placed at either end of the columns. These boundary elements are used to set the appropriate initial fluid conditions and 2 MPa pore pressure differential imposed between the top and bottom of the samples. The top and bottom boundaries are set to constant pressures of 52 and 50 MPa, respectively. Distilled water is used for the initial fluid. A drawback of using TOUGHREACT to simulate the flow-through experiments is that the code assumes open injection of the fluid (i.e., a fluid of constant composition is injected into the sample from the top boundary cell). However, the experiments were closed-loop (i.e., the same volume of fluid was cycled back and forth through the samples). To account for the recycling of fluid in the experiments, the constant pressure boundaries in TOUGHREACT were reversed at set intervals (listed in Table 2) and the chemistry of the injection fluid was updated to that of the outgoing fluid. The intervals for the flow reversals depend on flow rates. Initial reversal times were set to 10,000 seconds in all the models. The reversal times reported in Table 2 were determined by increasing or decreasing the reversal time until modeled profiles of aqueous species concentration, mineral abundance, and permeability approximated the experimental data. The flow rates in the lowest permeability samples (i.e., the intact samples and 250f-1, permeabilities listed in Table 1) required longer intervals between reversals to allow time for the injected fluid to move through the fracture. We note that we do not expect a direct match between the reversal times used in the simulations and the time intervals used by Morrow et al. [2001]. The reason for this is that in the experiments, fluid could be collected and stored between reversals within the pressure vessel without any loss of dissolved species. In TOUGHREACT, distilled water is injected into the system and as fluid flows out any species that have dissolved into solution are lost. To prevent flushing of solutes, we replicate fluid collection and storage by adjusting the reversal timings to maintain solute concentrations high enough to support mineral precipitation (i.e., changes of mineral abundances similar to those reported in the experiments) and permeability reduction.

Porosity estimates are not reported by Morrow et al. [2001]; however, Westerly granite has very low porosity (< 1%). In this study, we have assumed an initial bulk porosity of 0.9% (for simulations of 300f, 250f-2, and 250f-1 using variable *n*) or 0.1% (for simulations of 300i, 250i, 150i, and 250f-1 using constant *n*). The initial values for bulk permeability were set based on the experimental measurements. The primary and secondary minerals considered in the simulations are consistent with experimental observations and consist of plagioclase, K-feldspar, quartz, biotite, smectite, calcite, and zeolite (Table 3). Due to limited thermodynamic and kinetic data, we approximate the chemical and physical properties of plagioclase feldspar and biotite by resolving these minerals into their corresponding end-member components of albite and anorthite and annite and phlogopite, respectively [Johnson et al., 1998; Xu et al., 2004b]. Zeolite is represented by wairakite in the model. The thermodynamic data for all the minerals except smectite were taken from the TOUGHREACT database. The parameters for a high-Fe smectite were taken from the LLNL database [Delany and Lundeen, 1990]. Dissolution and precipitation of all minerals was assumed to be kinetically controlled using the rate law given in Eq. (4). The values for the rate constant at 25 °C (k_{25}) and the activation energy (E_a) were taken from published scientific literature. The same kinetic parameters are used for dissolution and precipitation. The modeled mineral phases, initial mineral volume fractions and reactive surface areas, and kinetic parameters are listed in Table 3. Assigning initial reactive mineral surface area is challenging. Because our main purpose is to investigate the temporal evolution of reactive surface areas and evaluate its relative importance to system evolution, we follow the approach of Xu and Pruess [2001] and assume a general reactive surface area of 1000 $cm^2\ g^{-1}$ in fractured granite and 100 $cm^2\ g^{-1}$ in intact granite (the lower value takes into account the fact that mineral surfaces may be less accessible to fluid in a granite matrix than a fracture). The initial areas of the primary minerals were then calculated by multiplying this surface area by the volume fractions reported in Table 3. Decreasing reactivity (i.e., less accessible reactive surface area) is modeled over time using Eq. (8).

Although the model outlined above is a simplified representation of the experiments, it nevertheless is useful for isolating the effects of surface area on alteration in fractured rock. Additionally, the physical and chemical parameters used in a one-dimensional, single-continuum reactive transport simulation are

Table 2: Timing of fluid flow reversals used in the simulations and values for the fitting parameters.

Experiment Name	Reversal Timing (s)	Fitting Parameters[a,b] n	m	M
150i	40000	5	–	–
250i	40000	5	–	–
250f-1	50000	–	4.0	2.0/3.0
250f-2	1000	–	4.0	2.0/3.0
300i	40000	5	–	–
300f	1000	–	4.0	2.0/3.0

[a] Intact samples use a constant n.
[b] For fractured samples, n is calculated using Eq. (10).

innately averaged and reflect the bulk properties of the medium being simulated. Because the values given by Morrow et al. [2001] are also for the bulk media, an approach utilizing bulk-media parameters may prove useful. However, we acknowledge that one-dimensional simulations do not address all the processes involved in controlling changes in the system. Permeability evolution is controlled by additional factors such as pore size distribution and localized precipitation and dissolution. In a two-dimensional model for flow within a fracture, for example, flow can migrate around asperity bridges or blocked pathways. Considerations such as these are not addressed in the current model. However, at this point, the immediate goal is to (i) explore the ability of a one-dimensional model to replicate observations from experiments conducted on fractured granite under various hydrothermal conditions and (ii) provide an initial evaluation of the relative importance of physical occlusion of reactive surface area by secondary precipitates (armoring) on system evolution. Comparison of this work with two-dimensional models should help to understand THC processes in a more mechanistic or process-based fashion.

DISCUSSION OF SIMULATION RESULTS

The Effects of Physical Occlusion on System Evolution

The manner in which changes in reactivity are modeled has a notable effect on the physical and chemical evolution of the system. As discussed above, we assume that precipitation of clays within open pore space is the dominant mechanism by which reactive surface area would be reduced during an experiment. If we assume that the mineral surface area available to the fluid for reaction is unaffected by clay-mineral coatings (i.e., $n = 0$ in Eq. 8), then there is rapid precipitation which causes a large reduction in permeability over a very short time (Fig. 1, arrow) and a spike in solute concentrations. This situation clearly does not match the experimental data. In general, the evolution pathway of a hydrothermal system is governed by a delicate

Table 3: Initial mineral volume fractions, surface areas, and kinetic properties used in the simulations.

Mineral	Volume (%)	A_o[a,b] ($cm^2\ g^{-1}$)	k_{25} ($mol\ m^{-2}\ s^{-1}$)	E_a ($kJ\ mol^{-1}$)
albite	30	300	1.0×10^{-10}	67.8
anorthite	10	100	5.6×10^{-09}	67.8
k-feldspar	20	200	3.9×10^{-13}	38.0
quartz	30	300	4.3×10^{-14}	89.0
annite	5	50	2.2×10^{-11}	60.0
phlogopite	5	50	1.2×10^{-11}	60.0
smectite	0	1000	1.0×10^{-14}	58.6
calcite	0	1000	1.6×10^{-06}	41.8
wairakite	0	1000	2.0×10^{-12}	62.8

[a] Surface area for fractured granite.
[b] Surface areas are reduced by an order of magnitude for intact granite (see text for details).

balance between mineral dissolution and precipitation which are connected by a series of feedbacks. As shown below, if progressive occlusion of the reactive mineral substrate by clays is assumed, mineral precipitation and fluid composition are moderated and simulation results align much more closely with those of the flow-through experiments.

As a means of evaluating the effectiveness of mineral occlusion in governing system evolution, we simulated experiment 250f-1 (Table 1) using constant values of n equal to 2, 4, and 6. Figures (1)–(3) illustrate the effect of reactive surface area reduction on system evolution. Greater feedback between mineral surface area and reaction rates is indicated by higher values of n. Larger values of n can be considered to indicate that occlusion of the reacting minerals by clays is very effective at reducing the surface area, A_j, over time, which in turn slows dissolution/precipitation reactions (Eq. 4).

Rapid dissolution of the primary minerals occurs early in the simulation as distilled water is injected into the granite. Dissolution of albite, anorthite, K-feldspar, quartz, annite, and phlogopite releases Na, SiO_2, K, Ca, Fe, Al, and Mg into solution. Over time, smectite and calcite become oversaturated with respect to the pore fluid and begin to precipitate. By removing solutes from solution, mineral precipitation can promote continued disequilibrium and dissolution. For all values of n, but most notably for $n = 2$, smectite precipitates quickly increasing the abundance of smectite in the simulated system (Fig. 2). Rapid formation of smectite also drives a larger decrease in permeability (Fig. 1) and increasing concentrations of K, Al, and SiO_2 (Fig. 3). As K, Al, and SiO_2 concentrations increase, K-feldspar also becomes oversaturated and starts to precipitate. Decreasing concentrations of Ca are driven by continued high rates of calcite precipitation. Concentrations of Na, Mg, and Fe remain fairly stable, possibly indicating that biotite and albite dissolution are balanced by smectite precipitation. By the end of the simulation for which $n = 2$, there are obvious deviations between experimental and

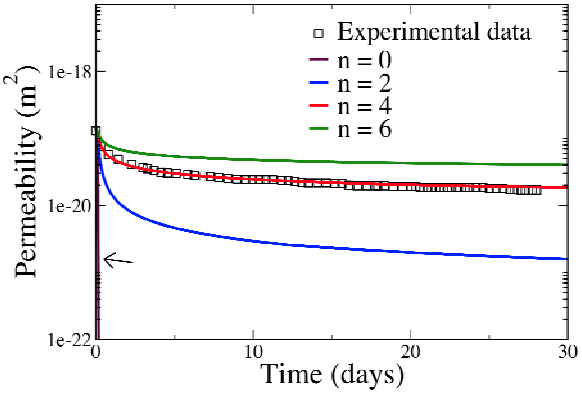

Figure 1: Permeability evolutions from simulations of 250f-1 using different values of n. The arrow highlights the rapid permeability decrease when n = 0. Squares indicate the permeability changes observed by Morrow et al. [2001] for experiment 250f-1.

simulation results. The most prominent differences are that the model permeability is too low (Fig. 1), the relative abundance of K-feldspar (Fig. 2) exceeds that observed in the experiment, and the simulated concentrations of K, Ca, and Al trend away from that of the measured fluid (Fig. 3). In making this last comparison, we assume that the final fluid composition of 250f-1 was similar to 250f-2 because 250f-2 is the only experiment for which aqueous chemical concentrations are reported.

A stronger feedback between surface area reduction and clay mineral precipitation (i.e., $n \geq 4$) better matches the observed mineralogy, fluid composition and permeability evolution (Figs. 1–3). Solute concentrations appear more stable, without large decreases or increases away from the final measured values. However, there is still appreciable lack of agreement between modeled and measured Na, SiO_2, and Al concentrations. Continued deviations between numerical and experimental results are likely due to a combination of factors such as the presence of saline pore fluid and/or salts in the granite cylinders that are not represented in the model [Moore et al., 1983], isomorphous substitution (i.e., the replacement of one ion by another) and cation release from smectite [Singer and Munns, 2006], and model conceptualization or assumptions (e.g., timing of flow reversal or smectite chemical composition).

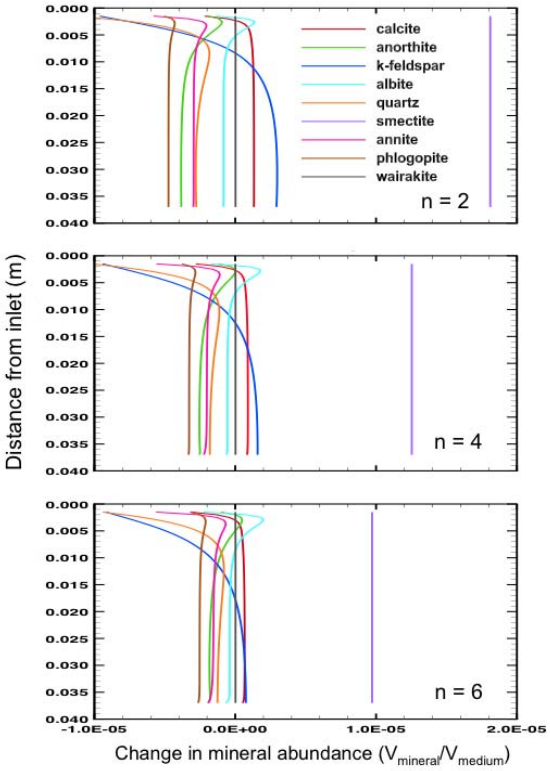

Figure 2: Changes of mineral abundances (volume fraction) in the simulations of 250f-1 using different values of n. Results reflect the final mineralogy after 28 days. Negative values indicate a decrease in mineral abundance.

Simulations of Fractured Samples

Many of the data for experiment 250f-1 were adequately modeled assuming progressive occlusion of the reactive mineral substrate by clays and using constant n values between 4 and 6. However, comparing simulations of 250f-1 (discussed above) with those for 250f-2 and 300f indicate that this approach may not apply generally for fractured granite. After an early phase of rapid permeability reduction, experimental measurements show that permeability continues to decrease more slowly. The continued decline in permeability is most evident in the higher permeability experiments 250f-2 and 300f and is not well reproduced by models using a constant n in Eq. (8) (as shown in the top panel of Fig. 4). In the case of constant $n > 4$, permeability reaches a fairly stable value after a few days, since reaction rates, r_m, are quickly driven to zero by the strong effect of clay precipitation on surface area reductions. This produces an essentially constant permeability at later stages. This "over-flattening" is

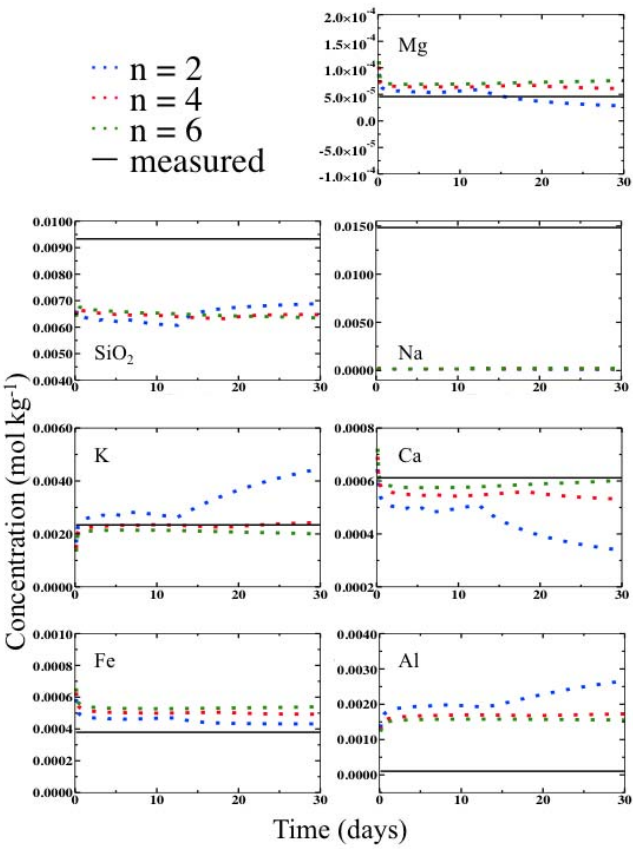

Figure 3: Evolution of fluid chemistry in simulations of 250f-1 using different values of n. Dashed lines indicate model results. Solid lines indicate the final pore-fluid chemistry measured by Morrow et al. [2001] for experiment 250f-2.

most obvious in Fig. (1) for n = 6 and Fig (4) (top panel). Nevertheless, as shown above a value of n between 4 and 6 is required to match the early evolution of the system. The problem may be that a larger, constant value of n overestimates the importance of surface area changes over time. It may be more realistic to assume that changes to reactive surface areas become less pronounced after an initial clay-mineral coating forms along the fracture surface.

To examine this effect, Equation (9) was incorporated into simulations of 250f-1, 250f-2, and 300f to evaluate the impact of progressively decreasing the feedback strength between smectite formation and surface area reduction. In the following simulations, the parameters l and m were set to 4 and 2/3, respectively. Since l and m are fitting parameters, these are not intrinsic values. The purpose of the parameters is to represent the physical process and significance of mineral occlusion in fractured rock. The selected values were determined numerically (i.e., they were adjusted until the simulation results approximated the data from all three experiments equally well). As previously mentioned, the selected values indicate the magnitude of the feedback between mineral surface area and reaction rates and the degree to which physical occlusion controls system properties. Adjusting the feedback between n and smectite abundance permits a slow continual decline in permeability that could not be captured in previous simulations using constant n in Eq. (8).

Comparison between the top and bottom panels in Fig. (4) shows that, overall, the model permeability curves using Eq. (9) better fit the data for all three experiments on fractured granite, although the improvement for the lowest permeability sample 250f-1 is small (c.f., Figs. 1 and 4). This approach produces mineral compositions, fluid chemistries and permeability evolution curves that reasonably match the available experimental data for fractured granite. For example, final relative mineral abundances in the simulation of 250f-2 (Fig. 5) generally match the relative abundances reported for the corresponding experiment (mineral abundances are larger here then in Fig. 2 due to increased initial porosity). The fluid chemical composition for K, Mg, Fe, Ca, and Al are also in fairly good agreement with the fluid sample analyzed by Morrow et al. [2001] (Fig. 6). Specifically, the final simulated concentrations of K, Mg, Fe are very close to the measured values. Also, the concentrations of Ca and Al approximate the measured values fairly well and are trending in the right direction. The most obvious misfits between the numerical and experimental results are the SiO_2 and Na concentrations. As K-feldspar begins precipitating, SiO_2 is removed from solution and its concentration moves away from the measured value. In all the simulations, Na concentrations remain very low (close to zero). This may indicate that additional considerations or more information on experimental conditions are required.

Simulations of Intact Samples

Unlike the fractured samples (250f-1, 250f-2, and 300f), in which permeability continues to decline after an early rapid decrease, measured permeability in the intact granite (150i, 250i, and 300i) tends to be much more constant over time, particularly at lower temperatures (Fig. 7). Using Eq. (9) to model the evolution of intact granite overestimates permeability reduction. Instead, the physical and chemical evolution of intact granite samples appears to be better modeled using constant n = 5. However, directly evaluating simulations of 150i, 250i and 300i is challenging since the secondary mineralogies and fluid composition reported by Morrow et al. [2001]

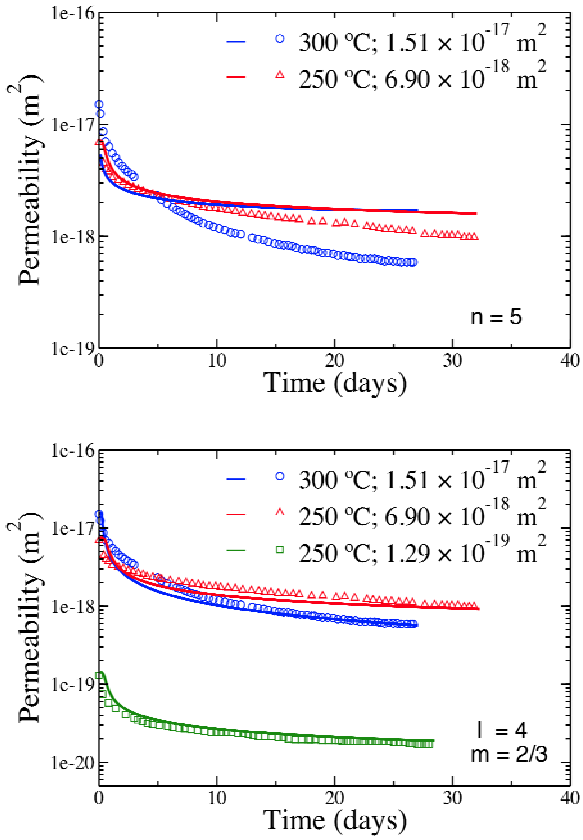

Figure 4: Evolution of permeability in fractured granite (250f-1, 250f-2 and 300f). Blue, red, and green lines correspond to experiments 300f, 250f-2, and 250f-1, respectively. Solid lines correspond to model results. Symbols are used to indicate the permeability changes observed by Morrow et al. [2001]. The top panel shows that simulation results fail to match the data from higher permeability experiments when constant n is used in Eq. (8). The lower panel shows the improved fit using Eq. (9) with l = 4 and m = 2/3.

are only for fractured granite.

Some insight still may be gained by comparing the simulations of intact granite to the fractured granite data. For example, concentrations of Mg, K, Ca, and Fe in the simulation of 250i are very close to those measured at the end of experiment 250f-2 (Fig. 8). However, as also seen in the simulation of 250f-2 (Fig. 6), SiO_2 and Na are lower than the experimental data. The low concentrations of Na and SiO_2 in all of the models suggest that the factors controlling fluid chemistry in fractured granite also apply to intact

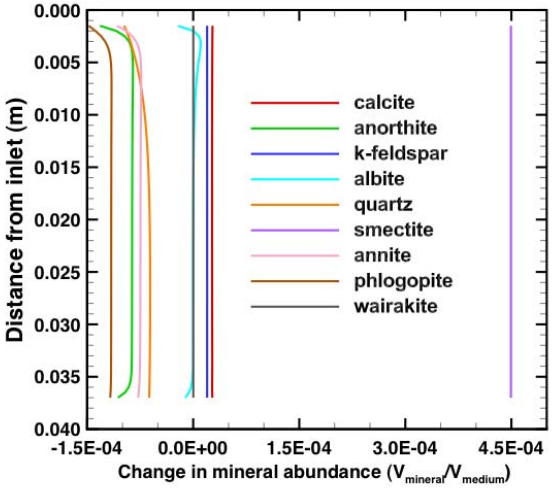

Figure 5: Change of mineral abundances (volume fraction) in the simulation of 250f-2 using Eq. (9) with l = 4 and m = 2/3 after 31.5 days.

samples. In general, the modeled fluid compositions of 250f-2 and 250i are similar, as expected since both models were run at the same temperature (250° C) and same starting mineralogy. The main distinction between the fractured and intact simulations is that solute concentrations for the intact sample 250i are predicted to reach their final values more rapidly than for the fractured sample 250f-2. This may reflect some combination of the longer reversal times (Table 2), constant *n* (leading to more rapid surface occlusion), and the smaller reactive surface areas and porosities used in the intact rock simulations.

Final mineral abundances in numerical simulations of 150i are dominated by smectite, K-feldspar, and albite (Fig. 9, lower panel). This is qualitatively similar to the relative proportions of mineral reaction products reported by Morrow et al. [2001] for fractured granite at 150 °C. Smectite, calcite, and albite are the major minerals that precipitated in the simulation of 250i (Fig. 9, upper panel). The obvious difference between the simulation results for 250i and the mineralogy reported from experiments on fractured granite at 250 °C is that no K-feldspar precipitates in the intact rock model; instead, K-feldspar dissolution is predicted along the entire length of the sample. This difference may be a further indication that the degree of saturation of the pore fluid with respect to K-feldspar is sensitive to the rate of smectite precipitation. As previously mentioned, dissolution of K-feldspar dominates early in the simulations of fractured granite. However, as the system evolves, smectite begins to precipitate, after which point K-feldspar precipitation is observed. Rates of smectite precipitation in 250i are slower than in 250f-2 and thus could explain the lack of K-

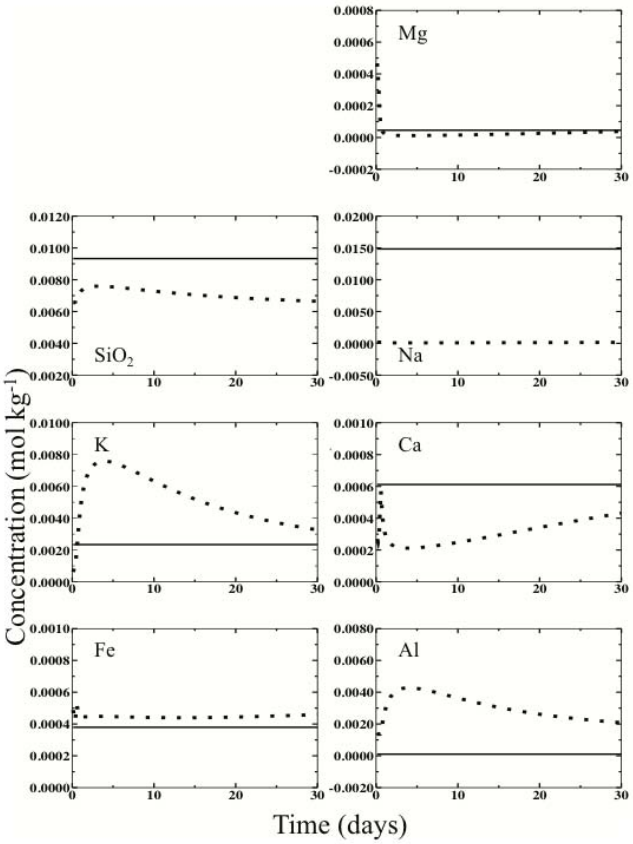

Figure 6: Evolution of fluid chemistry in the simulation of 250f-2. Dashed lines indicate model results using Eq. (9) with l = 4 and m = 2/3. Solid lines indicate the final pore-fluid chemistry measured by Morrow et al. [2001] for this experiment.

feldspar in simulations of the intact sample. Therefore, the simulation results for 250i are consistent with those for 250f-1 in that lower rates of smectite precipitation correspond to decreased abundances of K-feldspar (Figs. 2 and 9).

Control of smectite precipitation on system evolution also may be reflected by the fact that simulations of intact samples require a value of *n* that is different from that used to model fractured samples. In fractures, mineral occlusion initially may be an important mechanism for controlling reaction rates. However, as clays line a fracture, this mechanism may become less important, as represented by decreasing *n* values. In the tight granite matrix of intact samples, surface area reduction effects may be less dramatic or important. In short, the two sets of *n* values required by the data may indicate that the mechanisms controlling system evolution behave differently in fractured and intact rock due to structural differences. These differences may be

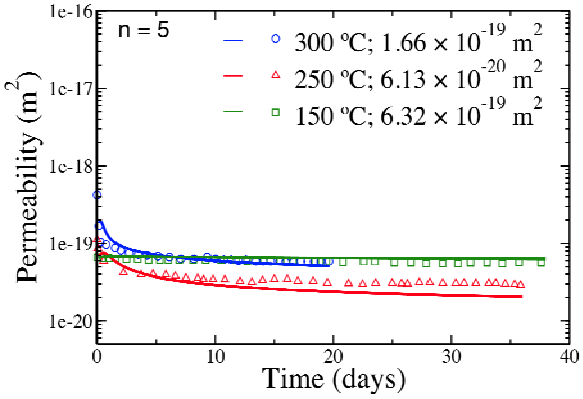

Figure 7: Evolution of permeability in intact granite (150i, 250i and 300i). Blue, red, and green lines correspond to 300i, 250i, and 150i, respectively. Solid lines correspond to model results using a constant n = 5. Symbols are used to indicate the permeability changes observed by Morrow et al. [2001].

resolved through the use of more complex or higher-dimension models.

SUMMARY AND CONCLUSIONS

This study was motivated by observations that mineral reaction rates decrease with time in both laboratory- and field-scale systems. Chemical or physical changes in mineral surfaces over time have been implicated as possible sources of this rate decrease. Consequently, reactive fluid flow through intact and fractured cylinders of Westerly granite was simulated to explore the effect of progressive surface area loss on system properties.

We find that dramatic deviations between model and experimental results occur when changes in reactive surface areas are not taken into account. When equations such as (8) and (9) are not employed in the models, reactions proceed too quickly. This causes a spike in solute concentrations and a rapid decrease in permeability that do not match experimental observations. In contrast, our simulations are capable of generating results that are qualitatively in good agreement with those of the experiments if Eq. (8) is implemented. The value of *n* in Eq. (8) can be either constant or change with smectite abundance according to Eq. (9). Whether a constant or changing *n* is more appropriate depends on the structure of the system being evaluated. Equation (9) represents a feedback between *n* and smectite abundance and captures the slow continual decline in permeability measured in flow-through experiments on fractured granite. A more stable permeability is observed for intact granite, which is best represented by a constant

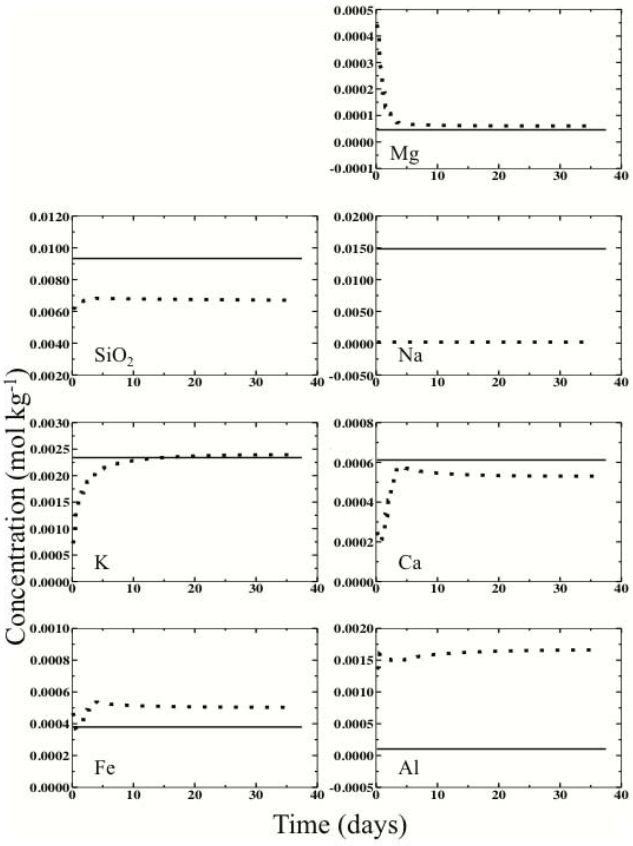

Figure 8: Evolution of fluid chemistry in the simulation of 250i. Dashed lines indicate model results using a constant n = 5. Solid lines indicate the final pore fluid chemistry measured by Morrow et al. [2001] for experiment 250f-2.

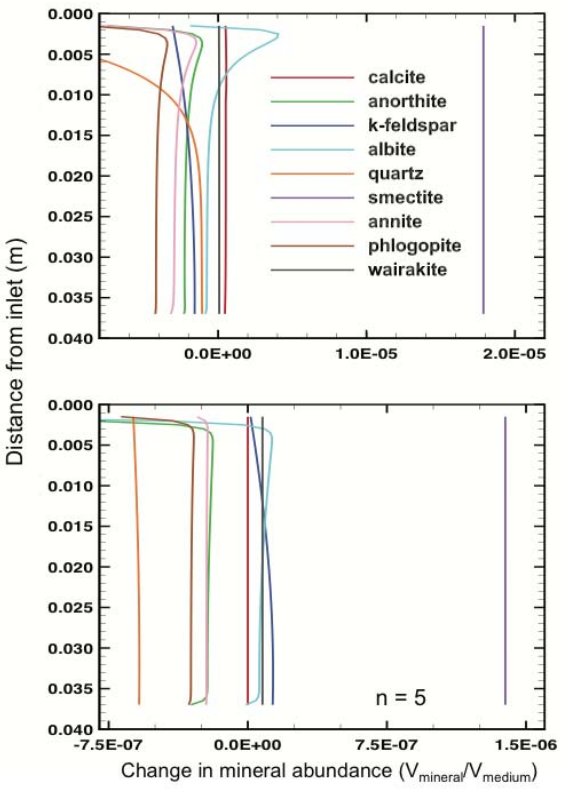

Figure 9: Change of mineral abundances (volume fraction) at the end of the simulations of 250i (upper panel) and 150i (lower panel) using a constant n = 5 for both samples and temperatures of 250° and 150° C, respectively. End times for 150i and 250i correspond to 37.5 and 35.6 days, respectively.

n. Overall, the simulation results seem to support the inference that gradual loss of reactive sites on silicate surfaces contribute significantly to the chemical and physical properties of granite under hydrothermal conditions. Thus, a method addressing changes in surface reactivity is necessary for accurate prediction of system behavior.

The modeling approach outlined in this paper is meant to represent mineral occlusion by clays and is successful under a variety of experimental conditions using a consistent set of values for the fitting parameters defined in Eqs. (8) and (9). The simulation results seem to validate this approach as a first approximation for predicting physical and chemical property changes in hydrothermal systems. However, because Eqs. (8) and (9) are not based on a first principle theory, the parameters *n*, *l*, and *m* are not strictly geometric or fundamental properties. Furthermore, although most of the experimental data on permeability, alteration mineralogy and fluid chemistry are well replicated in the models, concentrations of Na and, to a lesser extent, SiO_2 are not. This disagreement between the laboratory data and the model suggests that system property changes arise from additional processes or a more complex configuration than is considered here. For example, the only source of Na in the model is albite. Deviations in fluid chemistry between model and experiments could be partly due to saline pore fluid and/or salts present in the granite samples that were not included in the model. Another possibility is that the fixed chemical composition of the high-Fe smectite used in the model causes too much Na to be removed from solution. The chemical composition of the smectite formed in the experiments is unknown; however, the structure and composition of smectite depends on factors such as pore fluid chemistry, isomorphous substitution, and cation release. Therefore, it is unlikely that the smectite formed in the experiments is exactly the same as that assumed in the model. Spatial variations in pore geometry and

mineralogy due to localized precipitation or dissolution that are not treated in our 1-D model could also affect the chemical and physical properties of the system.

Although the simulation results do not entirely match experimental observations of mineral alteration, fluid chemistry, and permeability evolution, there is very close agreement in most respects. This provides some measure of confidence that the proposed model provides a framework for studying THC processes in fractured granite under hydrothermal conditions. The present model uses a relatively simple approach to relate the evolution of bulk physical and chemical system properties to mineral surface area changes. More advanced reactive transport models that build upon the model presented in this paper should broaden the scope and utility of this approach in the assessment of natural geothermal systems.

REFERENCES

Aagaard, P., and H. Helgeson (1982), Thermodynamic and kinetic constraints on reaction rates among minerals and aqueous solutions: I. Theoretical considerations, *Am. J. Sci.*, **282**, 237–285.

Alekseyev, V. A., L. S. Medvedeva, N. I. Prisyagina, S. S. Meshalkin, and A. I. Balabin (1997), Change in the dissolution rates of alkali feldspars as a result of secondary mineral precipitation and approach to equilibrium, *Geochim. Cosmochim. Acta*, **61**, 1125–1142.

Amrhein, C., and D. L. Suarez (1992), Some factors affecting the dissolution kinetics of anorthite at 25 °C, *Geochim. Cosmochim. Acta*, **56**, 1815–1826.

André, L., N. Spycher, T. Xu, K. Pruess, and F. D. Vuataz (2006), Comparing FRACHEM and TOUGHREACT for reactive transport modeling of brine-rock interactions in enhanced geothermal systems (EGS), in *Thirty-first Workshop on Geothermal Reservoir Engineering*, Stanford University, Stanford, CA.

Banfield, J. F., and W. W. Barker (1994), Direct observation of reactant-product interfaces formed in natural weathering of exsolved, defective amphibole to smectite: Evidence for episodic, isovolumetric reactions involving structural inheritance, *Geochim. Cosmochim. Acta*, **58**, 1419–1429.

Bethke, C. M. (1996), *Geochemical reaction modeling*, Oxford University Press, New York, 397 pp.

Brantley, S. L. (2003), Reaction kinetics of primary rock-forming minerals under ambient conditions, in *Treatise on Geochemistry*, vol. 5, edited by J. I. Drever, pp. 73–118, Pergamon Press, Oxford.

Brantley, S. L. (2008), Kinetics of mineral dissolution, in *Kinetics of water-rock interaction*, edited by S. L. Brantley, J. D. Kubicki, and A. F. White, pp. 151–210, Springer, New York.

Brantley, S. L., and C. F. Conrad (2008), Analysis of rates of geochemical reactions, in *Kinetics of water-rock interaction*, edited by S. L. Brantley, J. D. Kubicki, and A. F. White, pp. 1–37, Springer, New York.

Brantley, S. L., B. Evans, S. H. Hickman, and D. A. Crerar (1990), Healing of microcracks in quartz: Implications for fluid flow, *Geology*, **18**, 136-139.

Brantley, S. L., A. F. White, and M. E. Hodson (1999), Surface areas of primary silicate minerals, in *Growth, dissolution and pattern formation in geosystems*, edited by B. Jamtveit and P. Meakin, pp. 291–326, Kluwer Academic Publishing, Amsterdam.

Cama, J., J. Ganor, C. Ayora, and A. C. Lasaga (2000), Smectite dissolution kinetics at 80 °C and pH 8.8, *Geochim. Cosmochim. Acta*, **64**, 2701–2717.

Chester, F. M., J. P. Evans, and R. L. Biegel (1993), Internal structure and weakening mechanisms of the San Andreas fault, *J. Geophys. Res.*, **98**, 771-786.

Delany, J. M., and S. R. Lundeen (1990), The LLNL thermo-chemical database, *Lawrence Livermore National Laboratory Report*, UCRL-21658, Livermore, CA, 150pp.

Dorn, R. (1995), Digital processing of back-scatter electron imagery: A microscopic approach to quantifying chemical weathering, *GSA Bull.*, **107**, 725–741.

Dove, P. M. (1995), Chemical weathering rates of silicate minerals, in Kinetic and thermodynamic controls on silica reactivity in weathering environments, edited by A. F. White and S. L. Brantley, *Mineralogical Society of America*, Washington, D.C., pp. 236–290.

Emmanuel, S., and B. Berkowitz (2005), Mixing-induced precipitation and porosity evolution in porous media, *Adv. Water Res.*, **28**, 337–344.

Ganor, J., J. L. Mogollón, and A. C. Lasaga (1995), The effect of pH on kaolinite dissolution rates and on activation energy, *Geochim. Cosmochim. Acta*, **59**, 1037–1052.

Ganor, J., J. L. Mogollón, and A. C. Lasaga (1999), Kinetics of gibbsite dissolution under low ionic strength conditions, *Geochim. Cosmochim. Acta*, **63**, 1635–1651.

Gautier, J.-M., E. H. Oelkers, and J. Schott (2001), Are quartz dissolution rates proportional to B.E.T. surface areas?, *Geochim. Cosmochim. Acta*, **65**, 1059–1070.

Helgeson, H. C., W. M. Murphy, and P. Aagaard (1984), Thermodynamic and kinetic constraints on reaction rates among minerals and aqueous solutions. II. Rate constants, effective surface

area, and the hydrolysis of feldspar, *Geochim. Cosmochim. Acta*, **48**, 2405–2432.

Johnson, J. W., K. G. Knauss, W. E. Glassley, L. D. DeLoach, and A. F. B. Thompson (1998), Reactive transport modeling of plug-flow reactor experiments: quartz and tuff dissolution at 240 °C, *J. Hydrology*, **209**, 81–111.

Kieffer, B., C.F. Jové, E.H. Oelkers, and J. Schott (1999), An experimental study of the reactive surface area of the Fontainebleau sandstone as a function of porosity, permeability, and fluid flow rate, *Geochim. Cosmochim. Acta*, **63**, 3525–3534.

Lasaga, A. C. (1984), Chemical kinetics of water-rock interactions, *J. Geophys. Res*., **89**, 4009–4025.

Lasaga, A. C., and A. Lüttge (2003), A model for crystal dissolution, *Eur. J. Mineral.*, **15**, 603–615.

Maher, K., C. I. Steefel, D. J. DePaolo, and B. E. Viani (2006), The mineral dissolution rate condundrum: Insights from reactive transport modeling of U isotopes and pore fluid chemistry in marine sediments, *Geochim. Cosmochim. Acta*, **70**, 337–363.

Martin, J. T., and R. P. Lowell (1997), On thermoelasticity and silica precipitation in hydrothermal systems: Numerical modeling of laboratory experiments, *J. Geophys. Res*., **102**, 12,095– 12,017.

Moore, D. E., C. A. Morrow, and J. D. Byerlee (1983), Chemical reactions accompanying fluid flow through granite held in a temperature gradient, *Geochim. Cosmochim. Acta*, **47**, 445–453.

Moore, D. E., D. A. Lockner, and J. D. Byerlee (1994), Reduction of permeability in granite at elevated temperatures, *Science*, **265**, 1558–1561.

Morrow, C. A., D. E. Moore, and D. A. Lockner (2001), Permeability reduction in granite under hydrothermal conditions, *J. Geophys. Res.*, **106**, 30,551–30,560.

Nagy, K. L., and A. C. Lasaga (1992), Dissolution and precipitation kinetics of gibbsite at 80 °C and pH 3: The dependence on solution saturation state, *Geochim. Cosmochim. Acta*, **56**, 3093–3111.

Nagy, K. L., A. E. Blum, and A. C. Lasaga (1991), Dissolution and precipitation kinetics of kaolinite at 80 °C and pH 3: The dependence on solution saturation state, *Am. J. Sci*., **291**, 649–686.

Narasimhan, T. N., and P. A. Witherspoon (1976), An integrated finite difference method for analyzing fluid flow in porous media, *Water Resour. Res*., **12**, 57–64.

Nugent, M. A., S. L. Brantley, C. G. Pantano, and P. A. Maurice (1998), The influence of natural mineral coatings on feldspar weathering, *Nature*, **395**, 588–591.

Palandri, J., and Y. K. Kharaka (2004), A compilation of rate parameters of water-mineral interaction kinetics for application to geochemical modeling, *U. S. Geol. Surv. Open File Rep*. 2004-1068, p. 64pp.

Peters, C. A. (2009), Accessibilities of reactive minerals in consolidated sedimentary rock: An imaging study of three sandstones, *Chem. Geol*., **265**, 198–208.

Pruess, K. (1991), TOUGH2: A general numerical simulator for multiphase fluid and heat flow, *Lawrence Berkeley National Laboratory Report*, Rep. LBL-29400, Berkeley, CA, 37pp.

Singer, M. J., and D. N. Munns (2006), *Soils: An introduction*, 6th ed., Pearson-Prentice Hall, New Jersey.

Snow, D. T. (1968), Rock fracture spacings, openings, and porosities, *Proceedings Am. Soc. Civ. Eng.*, **94**, 73–91

Sonnenthal, E., and P. J. Ortoleva (1994), Numerical simulations of overpressured compartments in sedimentary basins, in Basin compartments and seals, vol. 61, pp. 403–416, *AAPG Memoir*, Tulsa, OK.

Steefel, C. I. (2001), Software for modeling multicomponent, multidimensional reactive transport, *Lawrence Livermore National Laboratory Report*, UCRL-MA-143182, Livermore, CA.

Steefel, C. I., and A. C. Lasaga (1994), A coupled model for transport of multiple chemical species and kinetic precipitation/dissolution reactions with applications to reactive flow in single phase hydrothermal system, *Am. J. Sci*., **294**, 529–592.

Steefel, C. I., D. J. DePaolo, and P. C. Lichtner (2005), Reactive transport modeling: An essential tool and a new research approach for the Earth sciences, *Earth Planet. Sci. Lett*., **240**, 539–558.

Stillings, L. L., and S. L. Brantley (1995), Feldspar dissolution at 25 °C and pH 3: Reaction stoichiometry and the effect of cations, *Geochim. Cosmochim. Acta*, **59**, 1483–1496.

White, A. F., and S. L. Brantley (Eds.) (1995), Chemical weathering rates of silicate minerals, vol. 31, *Mineralogical Society of America*, Washington, D.C.

White, A. F., and S. L. Brantley (2003), The effect of time on the weathering of silicate minerals: Why do weathering rates differ in the laboratory and field?, *Chem. Geol*., **202**, 479–506.

White, A. F., and M. L. Peterson (1990), Role of reactive surface area characterization in geochemical models, in *Chemical Models of Aqueous Systems*, vol. 2, pp. 461–475, Am. Chem. Soc., Washington, D.C.

Xu, T., and K. Pruess (1998), Coupled modeling of non- isothermal multiphase flow, solute transport and reactive chemistry in porous and fractured media: 1. Model development and validation,

Lawrence Berkeley National Laboratory Report, LBNL-42050, Berkeley, CA, 38pp.

Xu, T., and K. Pruess (2001), On fluid flow and mineral alteration in fractured caprock of magmatic hydrothermal systems, *J. Geophys. Res.*, **106**, 2121–2138.

Xu, T., F. Gérard, K. Pruess, and G. Brimhall (1997), Modeling non-isothermal multiphase multi-species reactive chemical transport in geologic media, *Lawrence Berkeley National Laboratory Report*, REP. LBNL-40504, Berkeley, CA, 79pp.

Xu, T., E. Sonnenthal, N. Spycher, K. Pruess, G. Brimhall, and J. Apps (2001), Modeling multiphase non-isothermal fluid flow and reactive geochemical transport in variably saturated fractured rocks: 2. Applications to supergene copper enrichment and hydrothermal flows, *Am. J. Sci.*, **301**, 34–59.

Xu, T., E. Sonnenthal, N. Spycher, and K. Pruess (2003), Using TOUGHREACT to model reactive fluid flow and geochemical transport in hydrothermal systems, in *GRC Annual Meeting*, Morelia, Mexico.

Xu, T., E. Sonnenthal, N. Spycher, and K. Pruess (2004a), TOUGHREACT user's guide: A simulation program for non-isothermal multiphase reactive geochemical transport in variably saturated geologic media, *Lawrence Berkeley National Laboratory Report*, LBNL-55460, Berkeley, CA, 192pp.

Xu, T., J. A. Apps, and K. Pruess (2004b), Numerical simulation of CO2 disposal by mineral trapping in deep aquifers, *Appl. Geochem.*, **19**, 917–936.

Yasuhara, H., and D. Elsworth (2006), A numerical model simulating reactive transport and evolution of fracture permeability, *Int. J. Numer. Meth. Geomech.*, **30**, 1039–1062.

Zhu, C. (2005), In situ feldspar dissolution rates in an aquifer, *Geochim. Cosmochim. Acta*, **69**, 1435–1453.